TITLE

Control of asteroid retrieval trajectories to libration point orbits

AUTHOR NAMES AND AFFILIATIONS

Matteo Ceriotti
School of Engineering
University of Glasgow
G12 8QQ
Glasgow, United Kingdom
matteo.ceriotti@glasgow.ac.uk
Phone: +44 (0)141 330 6465
(Corresponding author)

Joan Pau Sanchez
Space Research Centre
Cranfield University
MK43 0AL
Bedfordshire
United Kingdom
jp.sanchez@cranfield.ac.uk
Phone: +44 (0) 1234750111

ABSTRACT

The fascinating idea of shepherding asteroids for science and resource utilization is being considered as a credible concept in a not too distant future. Past studies identified asteroids which could be efficiently injected into manifolds which wind onto periodic orbits around collinear Lagrangian points of the Sun-Earth system. However, the trajectories are unstable, and errors in the capture maneuver would lead to complete mission failure, with potential danger of collision with the Earth, if uncontrolled. This paper investigates the controllability of some asteroids along the transfers and the periodic orbits, assuming the use of a solar-electric low-thrust system shepherding the asteroid. Firstly, an analytical approach is introduced to estimate the stability of the trajectories from a dynamical point of view; then, a numerical control scheme based on a linear quadratic regulator is proposed, where the gains are optimized for each trajectory through a genetic algorithm. A stochastic simulation with a Monte Carlo approach is used to account for different perturbed initial conditions and the epistemic uncertainty on the asteroid mass. Results show that only a small subset of the considered combinations of trajectories/asteroids are reliably controllable, and therefore controllability must be taken into account in the selection of potential targets.

Keywords: Asteroid, Retrieval, Control, Trajectory, Libration-point orbits, Transfer

MANUSCRIPT

1. INTRODUCTION

Recent studies have suggested that near-Earth asteroids (NEAs) could be harvested and exploited for resources [1]. It is in fact well known that some NEAs are potentially full of strategic resources for in-space utilization (e.g., future in-orbit construction of space components) or even precious metals that may find interest in terrestrial commodity markets [2]. Harvesting asteroids will without doubt be costly; however more and more space companies have shown interest in this idea, as the benefit might overcome the cost in a relatively near-term [3].

A scenario that seems, arguably, as directly borrowed from the sci-fi, that of a rendezvous with an asteroid, to lasso it and haul it back to Earth neighborhood, was recently announced as a mission concept under serious consideration by NASA[1]. However, evidences on the interest of the concept can also be found in the preceding growth of scientific output on the concept [4-8].

A scenario which was investigated in the last few years consists of modifying the NEA's orbit such as to capture it into a libration orbit of the Sun-Earth system [9] – halo, planar or vertical Lyapunov. The asteroid motion may then remain indefinitely on a periodic orbit near a libration point, which is relatively accessible from Earth, or alternatively transferred to other regions of the cislunar space (e.g., Moon orbit [7]).

Recently, García et al. [9] identified asteroids which could be injected into manifolds which wind onto periodic orbits around collinear Lagrangian points of the Sun-Earth system, by means of two low-cost capture maneuvers. However, it is known that the considered periodic orbits as well as the associated manifolds are highly unstable, and small errors in the capture maneuver would bring to departure of the asteroid from the reference trajectory in a short time. The intrinsic risk of this scenario is the possibility to divert the asteroid's trajectory in a way that it could impact the Earth.

This paper therefore aims to provide a more accurate account of the towing maneuver required to place an asteroid on a libration point orbit near the Sun-Earth L_1 or L_2 points. The paper investigates the optimal control of the towing spacecraft during two distinct phases: firstly, at Earth approach, when the asteroid is still far but slowly approaching the Earth following a stable invariant manifold trajectory; secondly, after the insertion into a target libration orbit, as station keeping is still necessary in order to keep the asteroid from drifting away and causing any potential concern for the Earth. By means of a Monte-Carlo analysis, we quantify the control margins necessary to ensure that the asteroid does not divert irreparably on a different trajectory, and hence becomes a risk for the Earth. In addition, a range of potentially useful target orbits near the libration points are analyzed in terms of station-keeping costs and safety.

In this paper, we will quantify the uncertainties of the state vector of the asteroid-spacecraft system, after the capture maneuvers, due to epistemic uncertainty on the mass of the asteroid. Given these perturbed states, a feedback control based on a linear quadratic regulator will be used to pilot a low-thrust engine to bring the system on the reference trajectory towards the final periodic orbit. A Monte Carlo approach will be used to generate a variety of different initial perturbed states and obtain some statistical results on the controllability of each combination of asteroid and trajectory.

[1] http://www.nasa.gov/sites/default/files/files/AsteroidRedirectMission_FS_508_2.pdf [retrieved 4 Sep 2013]

2. ASTEROID RETRIEVAL TRAJECTORIES

2.1. Equations of motion

The trajectories in this paper are modeled through the equations of motion of the normalized circular restricted three-body problem [10] (CR3BP) in a Sun-Earth synodic reference frame:

$$\begin{aligned} \ddot{x} &= 2\dot{y} + \frac{\partial \Omega}{\partial x} + \frac{T_x}{m} \\ \ddot{y} &= -2\dot{x} + \frac{\partial \Omega}{\partial y} + \frac{T_y}{m} \\ \ddot{z} &= \frac{\partial \Omega}{\partial y} + \frac{T_z}{m} \end{aligned} \tag{1}$$

with:

$$\Omega = \frac{x^2 + y^2}{2} + \frac{1-\mu}{r_S} + \frac{\mu}{r_E}$$

where $\mathbf{r} = \begin{bmatrix} x & y & z \end{bmatrix}^T$ is the position vector with respect to the origin in the synodic frame, r_S, r_E are the distances to the Sun and the Earth respectively and $\mu = 3.0032 \times 10^{-6}$ for the Sun-Earth system. $\mathbf{u} = \begin{bmatrix} T_x & T_y & T_z \end{bmatrix}^T$ is the control (i.e. thrust) vector, and *m* is the mass of the spacecraft and the asteroid, which are supposed to be tightly connected as a single point mass (Fig. 1a).

As is well known, when the thrust vector is zero, the system in Eqs. (1) has five equilibrium positions (see Fig. 1b). The Sun-Earth L_1 and L_2 points are of particular interest for us, since they are the *gate keepers* for potential ballistic capture of asteroids in the Earth's vicinity.

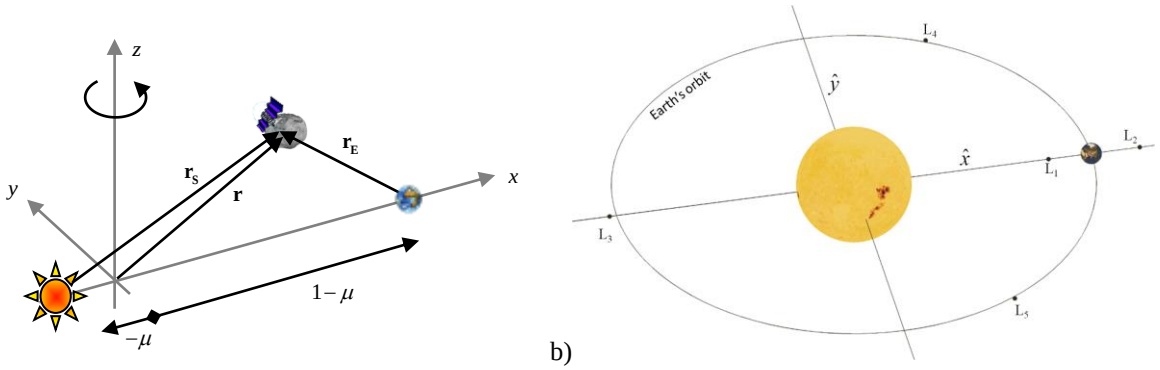

a) b)

Fig. 1. Schematic of (a) the CR3BP and (b) its equilibrium points.

The phase space near these equilibrium regions in the CR3BP can be divided into four broad classes of motion: bound motion near the equilibrium position (periodic orbit), asymptotic trajectories that approach or depart from the latter (hyperbolic manifolds), and other types of trajectories. In the planar case, the last can be classified as transit and non-transit trajectories [11] (see Fig. 2 for this division).

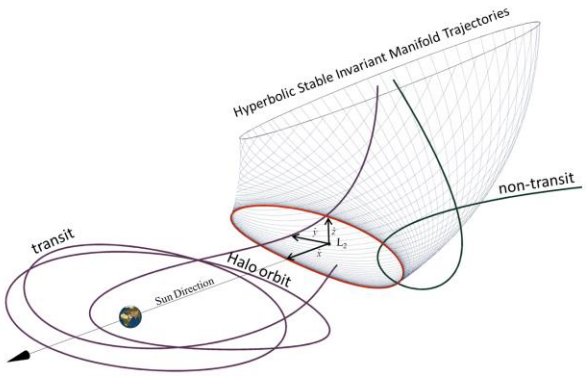

Fig. 2. Schematic representation of the four categories of motion near the L_2 point (represented by the set of axes in the figure): periodic motion around L_2 (i.e. halo orbit), hyperbolic invariant manifold structure (i.e. set of stable hyperbolic invariant manifold trajectories), and other types of trajectories.

2.2. Retrieval trajectories

Motivated by the recent interest on asteroids, and most particularly on the most accessible subset of its population, García et al. [9] carried out an exhaustive search for asteroids whose unperturbed trajectories laid close to an stable invariant manifold trajectories leading to one of the following distinct classes of periodic motion near the Sun-Earth L_1 and L_2 points: Planar (P), Vertical (V) Lyapunov and Halo Orbits north (Hn) and south (Hs).

Each of these families of libration point orbits (LPOs) is in fact a continuous set of periodic motion that can be explored by means of numerical continuation process with increasing Jacobi constant (i.e. energy). Fig. 3 shows a discretized set of Planar and Vertical Lyapunov orbits that cover Jacobi constants ranging from 3.0007982727 to 3.0000030032. Ticker red line corresponds to a Jacobi constant of 3.0004448196, which corresponds to half distance between the energy at equilibrium in L_2 and L_3.

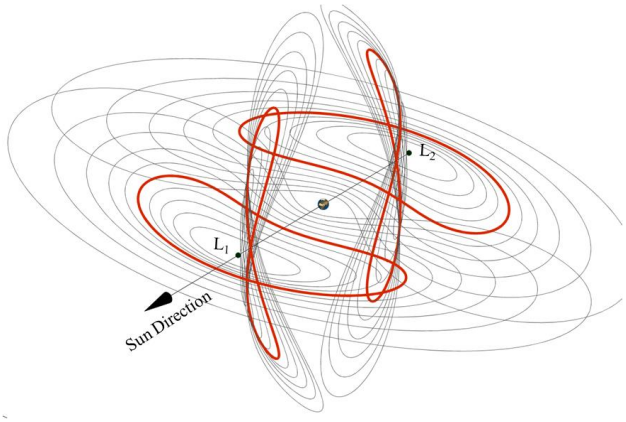

Fig. 3. Series of Planar and Vertical Lyapunov orbits associated with the Sun-Earth L_1 and L_2 points.

From each of these LPOs, a hyperbolic invariant stable manifold can be generated that consist of an infinite number of trajectories exponentially approaching the periodic orbit to which they are associated. A subset of invariant stable manifold trajectories, such as the one represented in Fig. 2, can be propagated backwards in the CR3BP framework for an arbitrary time.

In García et al. [9] these trajectories were propagated to a planar section located at a π/8 angle with the Sun-Earth line. This section corresponds roughly to a distance to Earth of the order of 0.4 AU, where the gravitational influence of the planet is considered small. Hence, from this section outwards, these trajectories could be well approximated in two-body motion, and thus described analytically by means of constant orbital elements. Note that the only exception the longitude of the perihelion, i.e. the sum of the right ascension of the ascending node and the argument of perihelion, which varies with a simple function of time due to the motion of the Earth on its orbit [9].
Finally, as depicted in Fig. 4, the sets of orbital elements associated with stable invariant manifold trajectories at the π/8 section form the basis for a *bullseye* orbit targeting that was solved as an heliocentric Lambert arc of a restricted two-body problem with two impulsive burns, one to depart from the NEO, the final one for insertion into the manifold, with the insertion constrained to take place before or at the ±π/8 section. These capture transfers can then be defined with 5 variables: the Lambert arc transfer time, the manifold transfer time, the insertion date at the target periodic orbit, the energy of the final orbit, and a fifth parameter determining the point in the target orbit where the insertion takes place; then, optimal transfer opportunities where found by a global stochastic search [9]. Table 1 summarizes the best trajectories found for each type of target orbit for L_2 and L_1.

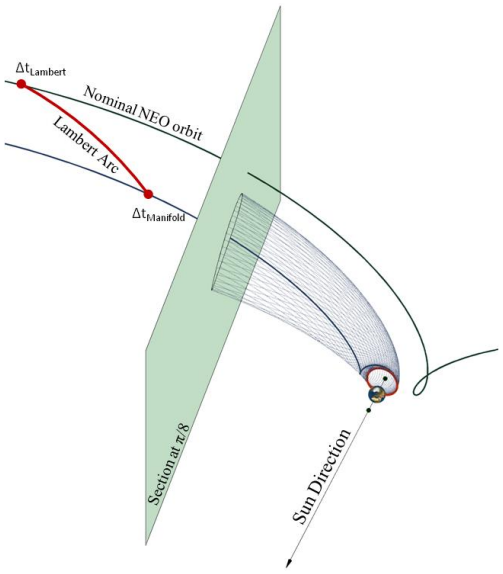

Fig. 4. Schematic representation of a transfer to L_2.

Despite the fact that the work presented in Ref. [9] also discusses the possibility that these trajectories could be flown, the conclusions were based solely on the transfer costs involved and the capability of current propulsion systems to provide the necessary change of linear momentum. This work, on the other hand, will deal with another critical issue with regards the feasibility of these trajectories; the controllability of the asteroid during the towing and parking process, in particular to avoid any unnecessary collisional risk with Earth or other human asset in space. Hence, the paper will attempts to provide further considerations on the feasibility of these trajectories by focusing on

the 8 transfers described in Table 1, which cover all types of periodic motion considered in García et al. [9] and [12][2].

Table 1. Asteroid reference trajectories.

	Asteroid name	Orbit destination	Date [yyyy/mm/dd]			Energy of Manifold	Total Duration [yrs]	Δv [m/s]		
			Asteroid departure	Manifold insertion	L_1 or L_2 arrival			Dep	Ins	Total
1.	2011 UD21	1Hn	2039/10/25	2040/06/16	2043/08/30	3.000504	3.85	210	225	436
2.	2011 UD21	1Hs	2037/11/22	2038/07/05	2042/07/18	3.000411	4.65	149	207	357
3.	2000 SG344	1P	2024/02/11	2025/03/11	2027/06/19	3.000357	3.35	195	248	443
4.	2011 UD21	1V	2036/07/20	2038/11/16	2041/06/21	3.000666	4.92	226	196	422
5.	2006 RH120	2Hn	2023/05/11	2024/02/20	2028/09/01	3.000548	5.31	52	55	107
6.	2006 RH120	2Hs	2021/02/04	2025/02/20	2028/08/05	3.000422	7.50	58	0	59
7.	2007 UN12	2P	2013/10/23	2016/11/29	2021/02/20	3.000069	7.33	199	0	199
8.	2010 VQ98	2V	2035/02/19	2036/10/06	2039/11/14	3.000017	4.74	177	4	182

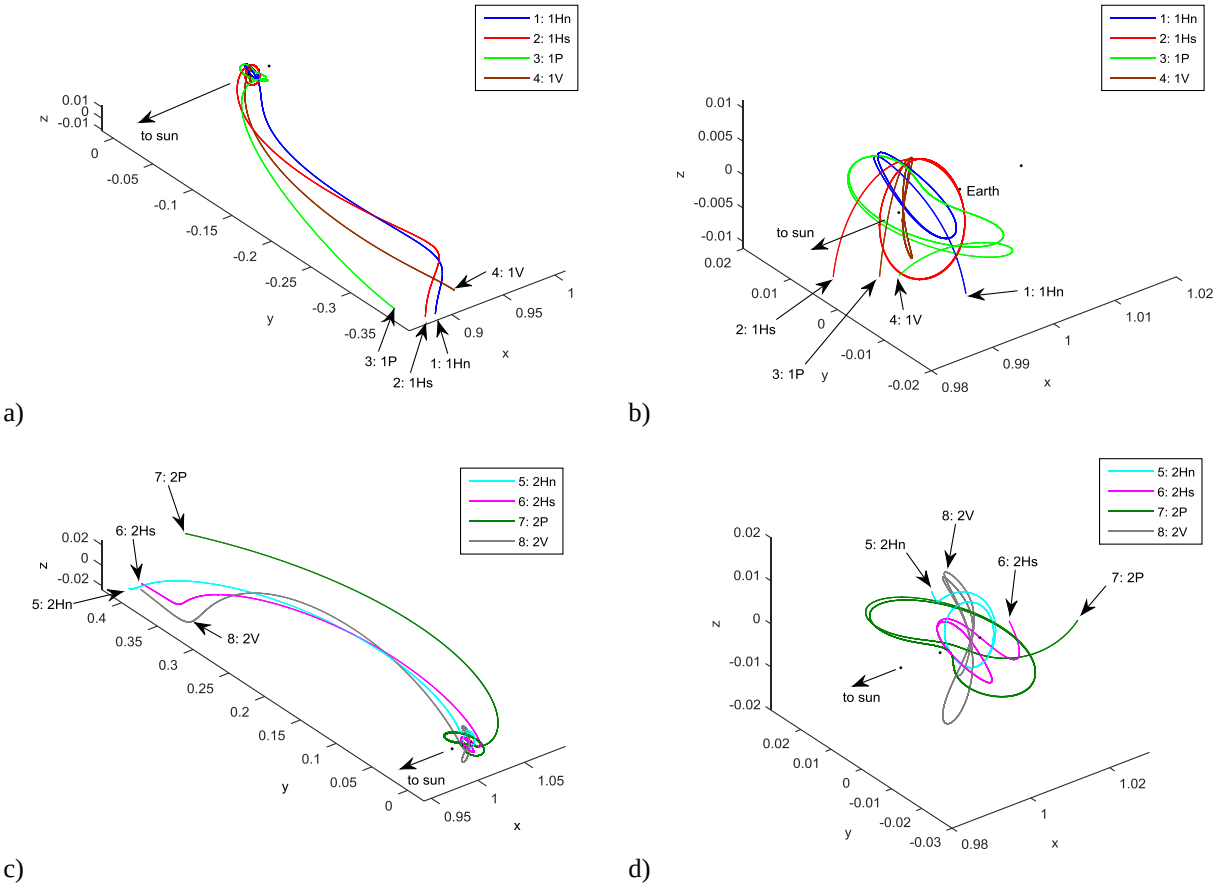

Fig. 5. Asteroid trajectories to periodic orbits considered. a) and b) are trajectories 1-4 to L_1, c) and d) are trajectories 5-8 to L_2.

Fig. 5 depicts these 8 capture trajectories. Two distinct parts compose these trajectories: the hyperbolic stable invariant manifold trajectory that approaches the equilibrium point and the periodic motion near the equilibrium point. These two parts are entirely ballistic trajectories, which, in the original work [9], were assumed to be flown

[2] Minor differences on some trajectories are due to numerical accuracy.

with negligible correction maneuvers. The 8 trajectories include also one complete period along their respective periodic orbit. It is here assumed that if it is possible to control the asteroid-spacecraft in the final part of the transfer and for one period of the periodic orbit, then further periods could also be controlled. All these trajectories will be used as reference in the following, for the feedback control algorithm.

2.3. Analytical study of the stability

It is well known that the collinear equilibrium points targeted by the capture trajectories in Table 1 are unstable equilibrium locations [13]. Hence, both the periodic orbits targeted by the asteroid and their associated hyperbolic stable manifold trajectories used to bring the asteroid near the Lagrange point will also be unstable. It is in fact partly because of this instability that these capture trajectories are advantageous in terms of the energy required to insert into the trajectory, as well as because they are ballistic, or naturally occurring [14].

It is precisely because of this instability that active control is required, or else any infinitesimal perturbation in the direction of the instability would cause the asteroid to drift away from the capture trajectory and completely miss the capture opportunity. Hence, a measure of the level of instability of these trajectories, i.e. how fast an infinitesimally perturbed trajectory departs from the exact capture trajectory, should provide some insights into how easily these trajectories can be controlled and hence the amount of acceleration necessary for the spacecraft to track it.

It is important to recall that the capture trajectories in Table 1 are composed by two distinct parts: the asteroid is first inserted into a hyperbolic stable invariant manifold that asymptotically winds into a periodic orbit, then it will keep following the periodic orbit. The stability of each part of the trajectories will be discussed in the following.

In a dynamical system such as the CR3BP, the difference between two neighboring trajectories with initial states $\mathbf{s}_0$ and $\mathbf{s}_0 + \delta\mathbf{s}_0$ can be efficiently propagated by means of an error state transition matrix, such as:

$$\delta\mathbf{s} = \boldsymbol{\Phi}\left(t, t_0\right)\delta\mathbf{s}_0, \tag{2}$$

where the state transition matrix (SSM) $\boldsymbol{\Phi}\left(t, t_0\right)$ is numerically integrated as:

$$\begin{aligned} \dot{\boldsymbol{\Phi}}\left(t, t_0\right) &= \mathbf{A}\left(t\right)\boldsymbol{\Phi}\left(t, t_0\right) \\ \boldsymbol{\Phi}\left(t_0, t_0\right) &= \mathbf{I} \end{aligned},$$

and $\mathbf{A}\left(t\right)$ is the matrix of partial derivatives of the system, or Jacobian matrix [15].

The stability of a periodic orbit can be assessed by analyzing the fundamental solution matrix, i.e. the monodromy matrix $\mathbf{M}$ [16], computed as the SSM $\boldsymbol{\Phi}\left(t\right)$ evaluated after one period, i.e. $\boldsymbol{\Phi}\left(T\right)$ [16].According to Floquet's theory, the periodic orbit is said to be stable if all the eigenvalues of the monodromy matrix $\lambda_{\mathbf{M},j}$ have absolute value equal or smaller than 1 [17], since this would ensure that given an initial deviation from the exact periodic solution, the deviation would not grow indefinitely with increasing time. One possible way to assess how quickly a deviation will grow is by looking into the largest real eigenvalue of the monodromy matrix $\mathbf{M}$. However, the basis formed by the eigenvectors of $\mathbf{M}$ is not orthonormal, and thus the vector associated with the maximum eigenvalue ($\max_j \left|\lambda_{\mathbf{M},j}\right|$) does not necessarily define the direction of maximum expansion. Instead, the basis formed by the eigenvectors of the quadratic form $\boldsymbol{\Phi}^T\boldsymbol{\Phi}$ does satisfy the orthogonality condition. Hence, an initial deviation $\Delta\mathbf{s}_0$ in the direction of the

eigenvector associated with the maximum eigenvalue of $\mathbf{M}^T\mathbf{M}$ ensures the maximum growth of the deviation. If we refer here as *expansion* the ratio $\|\Delta\mathbf{s}\|/\|\Delta\mathbf{s}_0\|$, the maximum expansion of $\|\Delta\mathbf{s}\|/\|\Delta\mathbf{s}_0\|$ is then equivalent to the spectral norm of the monodromy matrix $\mathbf{M}$ [18]:

$$\|\mathbf{M}\| = \sqrt{\max_j \left|\lambda_{\mathbf{M}^T\mathbf{M},j}\right|}\,, \tag{3}$$

where $\lambda_{\mathbf{M}^T\mathbf{M},j}$ is the *j*-th eigenvalue of the quadratic form of the monodromy matrix $\mathbf{M}^T\mathbf{M}$. The spectral norm will then convey a measure of how quickly a deviation will grow. This growth occurs at each period, and thus, for the sake of comparison among the trajectories, it is more appropriate to look at the ratio of this growth divided by the time it takes to occur, i.e. the period of the orbit, obtaining the following indicator:

$$\eta_{PO} = \sqrt{\max_j \left|\lambda_{\mathbf{M}^T\mathbf{M},j}\right|}\Big/T\,.$$

On the other hand, the hyperbolic stable invariant manifold trajectories (winding onto the periodic orbit of choice) are not characterized by any periodicity, at least in the initial part. Hence, in this case, the SSM $\mathbf{\Phi}(t,t_0)$ is used instead, which maps some initial deviations from the starting conditions $\mathbf{s}(t_0)$ into the deviations at a given time *t*, as in Eq. (2). These SSMs $\mathbf{\Phi}(t,t_0)$ are computed here as those mapping the starting conditions of each hyperbolic invariant manifold trajectory up to the final considered point (as in Table 1 and Fig. 5). Similarly then, the average expansion for the hyperbolic invariant manifold trajectories can be characterized through the indicator:

$$\eta = \sqrt{\max_j \left|\lambda_{\mathbf{\Phi}^T\mathbf{\Phi},j}\right|}\Big/(t-t_0)\,. \tag{4}$$

The indicators are plotted in Fig. 6 for each periodic orbit and full transfer, where higher values indicate less stable trajectories. It is important to underline that, due to the linear nature of this analysis, these results are intended only to provide some qualitative measure of the relative instabilities of the different transfers and target orbits. In particular, the indicator will progressively lose its meaningfulness as the reference trajectory gets longer. As an example of the information that can be extracted from this analysis, we can infer that trajectory 7 is highly unstable and therefore may be difficult to track or control, while trajectories 4 and 8 may comparatively be easier targets to control, since they have a lower instability. It is worth also to note that the average expansion of the hyperbolic trajectories η is one order of magnitude larger than that of the periodic orbits η_{PO}: this means that the critical part of the stability is dictated by the transfer part, and we can postulate that, if an asteroid can be controlled along the transfer, then it will be easily controllable along the corresponding periodic orbit.

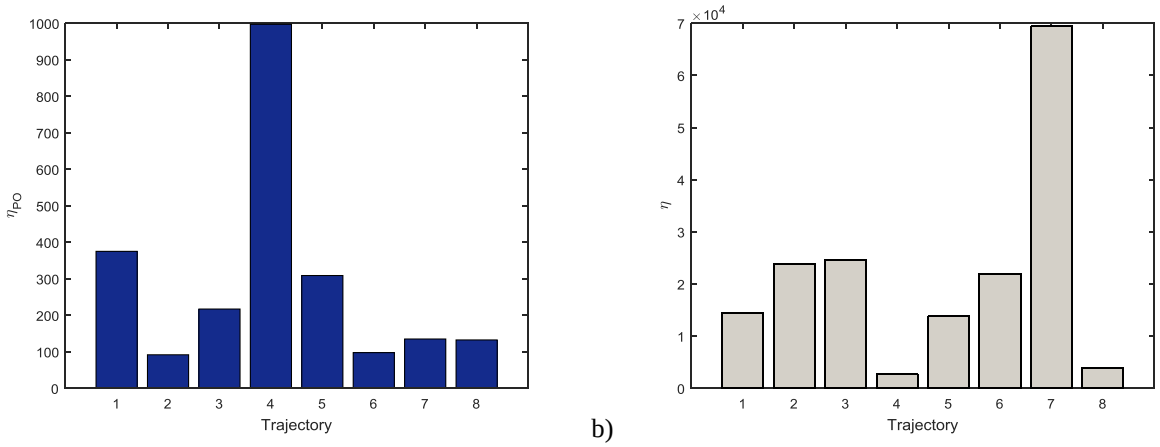

a) b)

Fig. 6. Stability indicators η_{PO} and η for a) periodic orbit, and b) full trajectory.

2.4. Uncertainty estimates for the manifold insertion

The trajectories in the previous subsection were computed assuming ideal conditions, i.e. all variables in the problem were exactly known. However, there are a number of uncertainties affecting the problem, the most important of which being the asteroid mass. In this work, we assume that the epistemic uncertainty on the mass of the asteroid to haul introduces an error on the velocity at the manifold insertion. While it is true that many other sources of error should be expected, such as inaccuracies on the thrust direction and magnitude, it is believed, as will be discussed below, that the single major source of uncertainty will be due to inaccuracies on the inertial mass of the object. Itokawa's mass measurements it is a good example of this issue [19]. Hayabusa spacecraft visited asteroid Itokawa during late 2005. An estimate of its mass was calculated to an accuracy of 3% by means of several different measurements of tracking and navigation data during different intervals. However, an asteroid retrieval mission will be expected a higher accuracy than that, since on addition to the remote measurements, a retrieval mission will be able to perform a series of initial pushing maneuvers to calibrate the system once the asteroid has been safely attached to the spacecraft. These initial maneuvers should increase considerably the accuracy of the mass of the system.

In this paper, nevertheless, we assume in 1% the epistemic error of the mass of target asteroid, after all measurement phase is completed, and thus, we study if such a mission could recover from that error at the insertion of the manifold trajectory.

Note however that we should distinguish between the residual epistemic uncertainty on the asteroid's mass by the time the asteroid retrieval phase is carried out and the lack of information available today on the asteroids in Table 1. The former is assumed to affect the reliability of a mission attempting to move an asteroid of a roughly known mass. The latter is only an added difficulty when attempting to make this analysis relevant to the asteroids in Table 1. In the fictitious scenario of an attempt to retrieve the asteroids in Table 1, a possible sequence of Earth remote observations, if opportunity arise, possible precursor missions, approaching phase of the retrieval spacecraft and final pushing maneuvers to calibrate the system should reduce the uncertainty of the mass of the asteroid to 1%, or lower.

Yet, the mass of the asteroid in Table 1 is today unknown, as happens with most of the asteroids, except for those that have been visited by a spacecraft or have a small companion orbiting it (i.e., binaries). Thus, it must be inferred from the only available information on the asteroid's physical characteristics: the absolute magnitude *H*. The mass can then be estimated as Ref. [20]:

$$m_{ast} = \frac{\pi}{6}\rho\left(\frac{1.329\cdot 10^6}{\sqrt{p_v}}10^{-H/5}\left[\mathrm{m}\right]\right)^3, \tag{5}$$

where ρ is the asteroid's density and p_v the albedo. Both ρ and p_v need to be assumed and average values for these two parameters are generally used [21]. Hence, due to plausible deviation from the average value of ρ and p_v, Eq. (5) provides only a rough estimate of the asteroid's mass that can easily be wrong by half an order of magnitude. Hence, as suggested in Ref. [22], this paper uses a mean value for $\rho\left(p_v\right)^{-3/2}$ based on the standard NEA (i.e., 43,000 kg/m^3) and minimum and maximum based on S-class asteroids (i.e. 35,000 kg/m^3) and M-class asteroids (i.e., 127,000 kg/m^3) respectively. Therefore, for each asteroid in Table 1, three possible masses were considered, which take into account the mean, minimum and maximum possible values.

2.4.1. Mass inaccuracies error propagation

If a particular asteroid transfer is expected to require a given change in velocity Δv_{tran}, we thus need to supply our system with a total change of linear momentum:

$$I_{tran} = \left(m_{ast} + m_{s/c}\right)\Delta v_{tran} \tag{6}$$

Or, by assuming I_{tran} as a requirement to follow the trajectory, we can rewrite:

$$\Delta v_{tran} = \frac{I_{tran}}{m_{ast} + m_{s/c}}.$$

By considering a small error in the asteroid mass δm_{ast}, and taking the differential of the previous equation, it is possible to relate it to the error in velocity change:

$$\delta\Delta v_{tran} = \frac{I_{tran}}{\left(m_{ast} + m_{s/c}\right)^2}\delta m_{ast},$$

Which, by substituting I_{tran} as in Eq. (6) and assuming that $m_{s/c}$ is negligible when compared with the mass of the asteroid m_{ast}, can be rewritten as:

$$\delta\Delta v_{tran} \approx \Delta v_{tran}\frac{\delta m_{ast}}{m_{ast}}.$$

Hence if 1% is the relative epistemic error of the mass of target asteroid, 1% is also the uncertainty in velocity. This 1%, however, is the uncertainty generated right after an impulsive maneuver. This error need to be propagated for the length of the transfer to account for the actual position and velocity uncertainty at the manifold insertion.

2.4.2. Definition of the perturbed initial states

The propagation based on the SSM, as described in Section 2.2.3 and Eq. (2) in particular, allows computing, at the time of the manifold insertion, the error in the states as a consequence of the capture trajectory. The errors in Table 2 were found, for each trajectory. These errors will be used as initial state errors for the following integration.

Table 2. Errors δs_0 on initial state vector.

		Position			Velocity	
Trajectory	km	km	km	km/s	km/s	km/s
1	127832	156409	15072	0.036	0.029	0.001
2	465252	196778	8855	0.043	0.097	0.002
3	215450	337688	6600	0.072	0.034	0.000
4	619108	445863	12655	0.095	0.117	0.003
5	89262	174744	2748	0.035	0.014	0.001
6	147144	221911	1190	0.042	0.030	0.001
7	198780	714752	3530	0.122	0.033	0.001
8	292209	83997	7849	0.012	0.060	0.001
Average	269380	291518	7313	0.057	0.052	0.001

As mentioned previously, the error on the mass of the asteroid-spacecraft system, is taken as 1% of the mass of the reference mass of asteroid.

The errors in Table 2 are used to generate the random initial states for the feedback control algorithm (see Fig. 7). A random normal distribution of points is generated, using the ellipsoid of uncertainty δs_i in Table 2 as 3σ:

$$s_i = s_{r,i} + \delta s_i \frac{\text{rndNorm}}{1.96}. \tag{7}$$

The index i refers to each one of the states, rndNorm is a randomly generated number following a normal distribution with zero mean and unitary standard deviation. The 1.96 normalization guarantees that the sample points are inside the ellipsoid of uncertainty, times the safety margin, with 97.5 % probability.

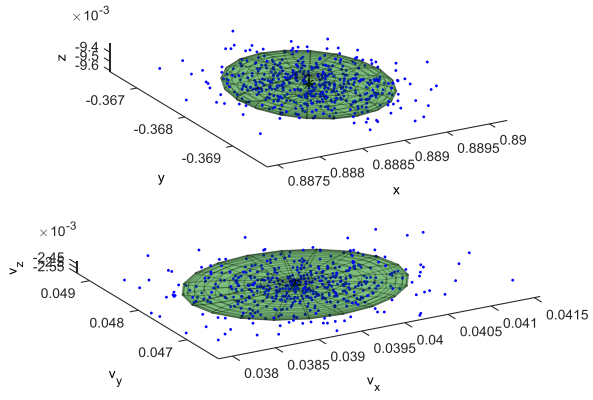

Fig. 7. Ellipsoids of uncertainty (3σ) for position and velocity, and 500 randomly sampled points for trajectory 1 (normalized units.).

3. MONTE CARLO APPROACH

A Monte Carlo method is used to assess the control of the asteroids on their respective trajectories, for a number of random initial conditions. The reference state is perturbed at the π/8 section in Fig. 4 (i.e. the beginning of the trajectories in Fig. 5a), where the controlled phase begins. This perturbation is modelling a different state in which the asteroid-spacecraft system might be, after the capture maneuvers, due to the uncertainty on the mass of the asteroid, as well as imperfections in the Δv delivery from the thruster.

The number of Monte Carlo points is selected such to have the (estimated) success rate p over N trials (see for example [23]). Fig. 8 plots the value of 3σ as function of p and for different N. For this work, we have decided to use N = 500 random points, such to get a 4% error at $p = 0.9$ and less than 7% at $p = 0.5$. The random points are generated using Eq. (7) for each trajectory.

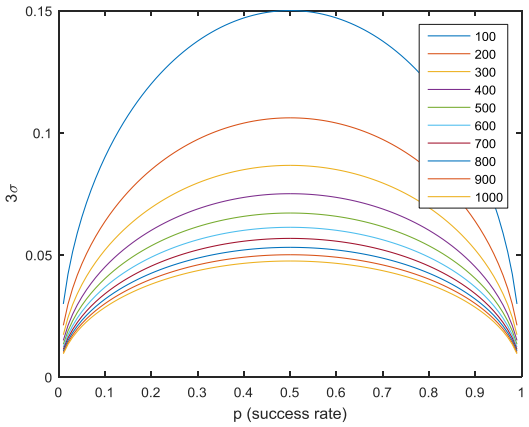

Fig. 8. Three-sigma function of the success rate *p*, for different numbers of trials *N*.

Fig. 9 shows a brief pseudo-code of the algorithm used to generate the sample points and run the control simulation on each one of them. Once each perturbed initial state is generated, the feedback control simulation is run, to assess whether it is possible to recover the spacecraft onto the reference trajectory. It is important to underline that the LQR optimal gains are recomputed for each trajectory and mass value.

```
For trajectory = 1, …, 8
  For mass = min, mean, max
    Optimize LQR gains with GA
    For point = 1…N
      Generate random initial state
      Run control simulation
      Check success
    End
  End
End
```

Fig. 9. Pseudo-code for the Monte Carlo simulation.

4. CONTROL SCHEME

Each perturbed initial state is propagated adding a feedback control with the aim to restore the reference conditions. The control loop used here is based on a linear quadratic regulator (LQR) [24], applied in a similar way as in Ceriotti et al. [25].

As actuator for the control loop, we assume to have a solar electric propulsion (SEP) thruster, whose characteristics are similar to the one considered by the NASA asteroid retrieval mission study [7]. In particular, the power available is $P_{SEP,max} = 40$ kW (here considered constant, not varying with the distance of the Sun) and the specific impulse is $I_{sp} = 3000$ s, from which the maximum thrust can be computed as:

$$T_{max} = 2P_{SEP,max}\eta_{SEP} / I_{sp} g_0 = 1.9 \text{ N} \tag{8}$$

where $\eta_{SEP} = 0.7$ is the efficiency of the SEP system [26] and $g_0 = 9.81$ m/s^2 is the standard gravity acceleration. The actual thrust that the thruster can deliver is continuously adaptable between 0 and T_{max} at any given time. It is also assumed that the thrust direction is not constrained, in the sense that the spacecraft (attached to the asteroid) has an attitude control system that is able to re-orient the nozzle in the direction of the required thrust. A control vector can therefore be defined as:

$$\mathbf{u} = \begin{bmatrix} T_x & T_y & T_z \end{bmatrix}^T$$

subject to the non-linear constraint $\|\mathbf{u}\| < T_{max}$.

For defining the control strategy, it is convenient to rewrite the equations of motion (1) as a first-order differential system $\dot{\mathbf{s}} = \mathbf{f}(t, \mathbf{s})$, including the mass, introducing the state vector $\mathbf{s} = \begin{bmatrix} x & y & z & v_x & v_y & v_z & m \end{bmatrix}$, where $\mathbf{v} = \dot{\mathbf{r}}$ and the dynamical equation of the mass change is:

$$\dot{m} = -u / I_{sp} g_0$$

Let us assume, at a given instant of time $\bar{t}$, that the spacecraft is at state $\mathbf{s}(\bar{t})$. At the same time, the reference state is $\mathbf{s}_r$ and the reference control is null, as the nominal trajectory is purely ballistic. The reference state defines the reference orbit as function of time, as discussed in the previous section. In an ideal condition, the real state coincides with the reference one. However, due to the instability of the trajectory and the uncertainty in the initial conditions, in general the real state may differ from the reference one, and therefore the state error can be defined as: $\delta\mathbf{s} = \mathbf{s} - \mathbf{s}_r$. The objective of the controller is to find the control $\mathbf{u}$ (defined as the feedback control) that brings the spacecraft states back to the reference states after some time.

To compute **u** at each instant of time, we use here a linear time-invariant approximation of the dynamical system. Due to this approximation, the real state shall be in the vicinity of the reference state. Furthermore, if we assume that the dynamics of the reference trajectory is slow enough, then we can approximate the time varying problem as a sequence of time-invariant problems, and use classic linear feedback control theory for computing the gain matrix. The optimal control problem is solved at each instant of time, and the gain matrix updated, as described in the following. It is not to be required to follow the mass state within the control: hence, the linearization is done in the following way:

$$\mathbf{A}_{6\times6}=\left.\frac{\partial\mathbf{f}}{\partial\mathbf{s}}\right|_{\mathbf{s}_r}\ ;\ \mathbf{B}_{6\times3}=\left.\frac{\partial\mathbf{f}}{\partial\mathbf{u}}\right|_{\mathbf{s}_r}$$

The derivatives of **f** with respect to states (except the mass) **A** and controls **B** are found analytically (their expression is omitted here), and then evaluated numerically. The dynamics of the system in the vicinity of $\mathbf{s}_r$ can then be expressed as:

$$\delta\dot{\mathbf{s}}=\mathbf{A}\delta\mathbf{s}+\mathbf{B}\mathbf{u} \tag{9}$$

This linear, time-invariant system approximates the real system at a given time and in the vicinity of the reference states. It can be verified through the controllability matrix that the system in Eq. (9) is controllable. However, non-linearities, as well as the saturation of the thrust, will limit the applicability of this method to some maximum displacement from the reference. The problem is now to find the optimal feedback control history $\mathbf{u}(t)$ for any time $t>\bar{t}$ such that the (linear) system of Eq. (9) will settle to the reference state, i.e. $\delta\mathbf{s}=0$. We introduce the following cost function:

$$J(\mathbf{u})=\int_0^\infty\left(\delta\mathbf{s}^T\mathbf{Q}\delta\mathbf{s}+\mathbf{u}^T\mathbf{R}\mathbf{u}\right)dt \tag{10}$$

which aims at minimizing the state error and the feedback control over an infinite amount of time, constrained to the linear system in Eq. (9). The matrices **Q** and **R** are weights that quantify the relative cost of each state and control in the cost function.

We now assume a control proportional to the state error, $\mathbf{u}=-\mathbf{K}\delta\mathbf{s}$. Minimizing Eq. (10) under this assumption leads to the well-known algebraic Riccati equation [24], which can be solved analytically to compute the gain matrix $\mathbf{K}_{3\times6}$.

The total control can then be computed, and saturation is applied according to the maximum thrust values presented in Eq. (8). The resulting thrust is then fed into the integration of the full equations of motion, including the mass flow. At the next time step in the integration, the procedure is restarted to update the feedback control: the gain matrix is computed dynamically during the simulation.

The choice of the matrices **Q** and **R** affects substantially the performance of the LQR, therefore an accurate selection of their coefficients is fundamental. An initial guess of their value was obtained initially following Bryson's rule (**Q**, **R** diagonal with Q_{ii} = maximum acceptable value of δs_i^2, R_{ii} = maximum acceptable value of u_i^2), and then the diagonal elements were optimized using a genetic algorithm (GA). The objective function (to be maximized) was selected being the success rate of 100 simulations with random initial conditions as described in Section 2.4.2. The GA optimization was repeated for each trajectory and asteroid mass, to guarantee the maximum success rate. Table 3 shows the values of the gains for each pair trajectory-mass value. Note that the values of the large exponents is due to the normalization of the CR3BP. In addition, the gains for mean and max mass of trajectory 3 were not computed as the success rate was zero for the minimum value of the mass already, and it cannot certainly increase for a more massive asteroid.

Table 3. Optimal LQR gains as found by the GA: a) Q_{ii} ×10^7, i = 1, 2, 3 (position); b) Q_{ii} ×10^4, i = 4, 5, 6 (velocity); c) R_{ii} ×10^{37}

Q_{ii} ×10^7, i = 1, 2, 3 (position)			
		Mass	
Trajectory	min	mean	max
1	8.0167	0.62945	3.4488
2	0.90608	9.1095	8.2364
3	0.34488	NaN	NaN
4	0.90679	0.65874	8.7437
5	0.81917	0.81917	0.24576
6	0.024635	0.26864	0.81917
7	5.0953	0.44360	6.4824
8	2.6046	0.90608	6.1974

Q_{ii} ×10^4, i = 4, 5, 6 (velocity)			
		Mass	
Trajectory	min	mean	max
1	1.9636	5.4320	0.14832
2	0.18459	1.8103	5.7191
3	6.8216	NaN	NaN
4	0.24673	0.014990	0.72607
5	0.70653	0.70653	0.85900
6	0.40916	0.26891	0.71955
7	0.50821	0.70653	0.20941
8	1.0405	0.11155	0.73491

R_{ii} ×10^{37}			
		Mass	
Trajectory	min	mean	max
1	1.8225	0.12196	0.10000
2	0.18881	1.5377	0.18881
3	0.010000	NaN	NaN
4	0.27899	0.11401	0.27838
5	0.24075	0.24075	0.13123
6	0.066908	0.52930	0.19028
7	17976	0.13538	0.26574
8	0.38939	0.15915	0.16652

4.1. Application to asteroid control

The control simulation runs for the time required for the reference trajectory to wind onto the periodic orbit and complete one period on it. After this time, the states of the simulation are compared with the states of the reference trajectory: if their distance is small (10^{-4} in position and 10^{-3} in velocity in normalized units), then the control is considered successful. Note that it was experienced that these tolerances are not affecting the results, in the sense that if the control is successful, then it very easily acquires the reference well below these tolerances; vice-versa, when the control is not sufficient, then the spacecraft diverges completely, causing a final separation from the reference that is of orders of magnitude greater than the tolerances.

Fig. 10a shows two controlled trajectories, starting from two different random points based on the same reference trajectory (namely trajectory 1, reference mass 341,697 kg): on one of them the control is successful, and in fact it is extremely close to the reference; the other trajectory, instead, diverges. The spacecraft does not get close to the reference for the whole manifold, for then departing considerably once on the periodic orbit.

For the successfully controlled solution, Fig. 10b shows the state error, i.e. the difference between the real state and the reference state, in terms of position and velocity. The same figure also shows the mass flow (considering 0 the

initial mass at the beginning of the controlled phase). This gives an estimation of the propellant mass required for the control of the asteroid during the transfer and one period around the orbit. Fig. 10c shows the required thrust in Cartesian components and magnitude. The trend is typical of an LQR controller, with a high amount of thrust at the beginning, to reduce the initial state error, and then some residual thrust to counterbalance the instabilities of the system.

In these plots, time is in the CR3BP conventional non-dimensional units, i.e. 1 year corresponds to 2π, and $t = 0$ corresponds to the insertion into the periodic orbit.

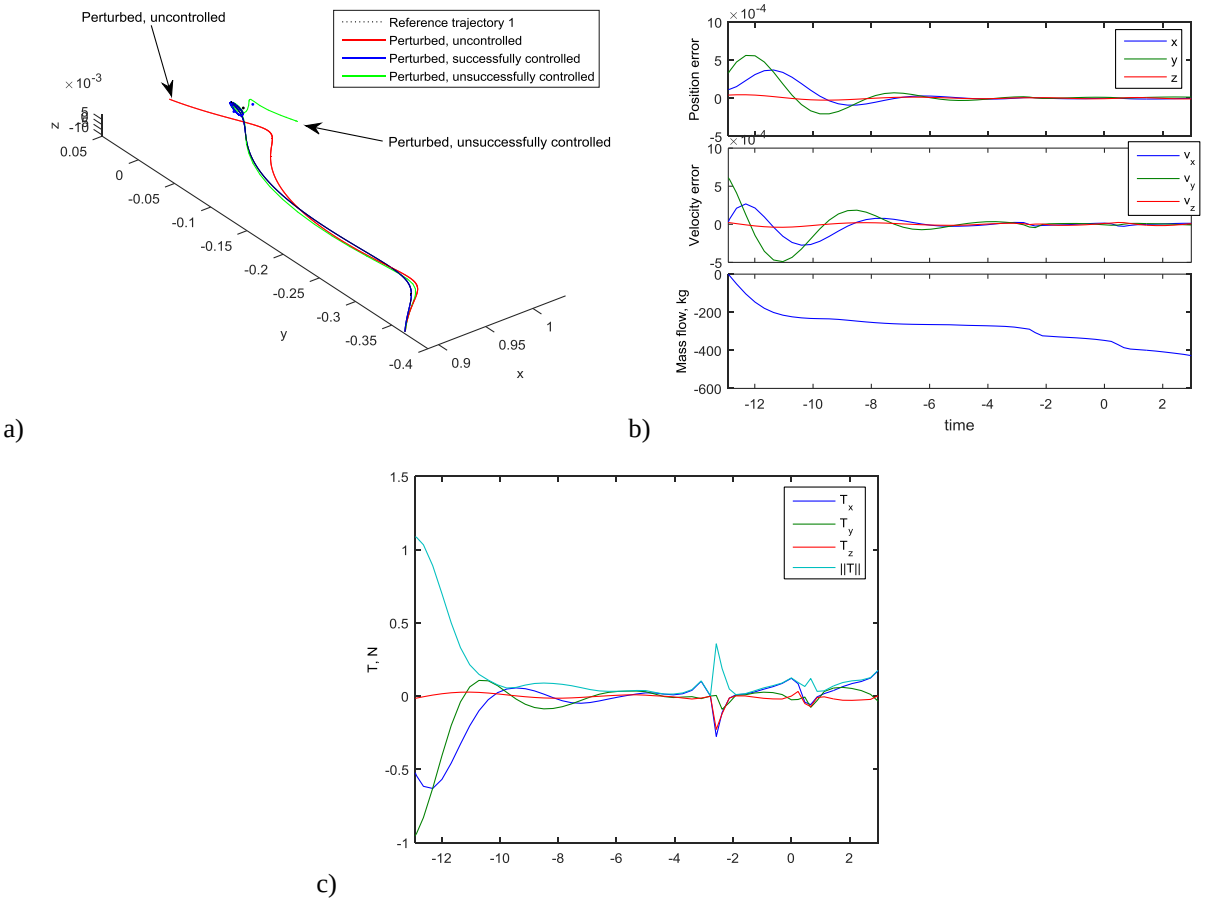

Fig. 10. (a) Two random initial states on trajectory 1 that lead to successful or unsuccessful control. (b) State error with respect to reference (position, velocity) and mass flow. (c) Control thrust.

5. RESULTS

The success rate for each trajectory and value of nominal mass is collected and shown in form of histograms in the following Fig. 11, showing the rate of success over the 500 simulations. Each plot refers to a trajectory, and contains three columns, each one referring to minimum, mean and maximum mass of the asteroid on that trajectory.

The first thing to note is that, because the thrust level is limited and unchanged for the different asteroids, the success rate is heavily affected by the mass of the asteroid. The acceleration that the thruster can provide is in fact inversely proportional to the mass of the system. For example, trajectory 3 is associated with a trajectory to retrieve asteroid

2000SG344, with a derived size ranging from 20 to 70 meters diameter. This object is by far the largest object that is considered for retrieval and, it is evident from Fig. 11, that the object would not be controllable with the assumed thrusting capability.

However, trajectory 1, 2 and 4 are associated with the same asteroid, 2011 UD21, and hence the spacecraft is carrying the same mass. Yet, the success rate of trajectory 1 is much higher than that of 2 and 4. It is therefore apparent that the asteroid's controllability does not solely depend on the mass of the object to be towed, but in many other factors, such as the type of LPO and energy that is targeted, the Δv of each maneuver, the lengths of the coasting arcs, etc. All this factors affect the controllability of these trajectories in conjunction, and is thus difficult to isolate their particular effects.

This dependence to many intertwined factors is evident, for example, in trajectories 5 and 6, which are associated with the smallest asteroid of the set, and indeed they have the highest success rates. Both of these trajectories target a Halo orbit, albeit one to the southern family and the other to the northern one. The stability of both families is expected to be similar, and hence both success rates are similar. However, it is noticeable that for trajectory 6 the success rate decreases consistently when considering the maximum mass, which does not happen for trajectory 5, for which the success rate is always above 98% regardless of the mass case.

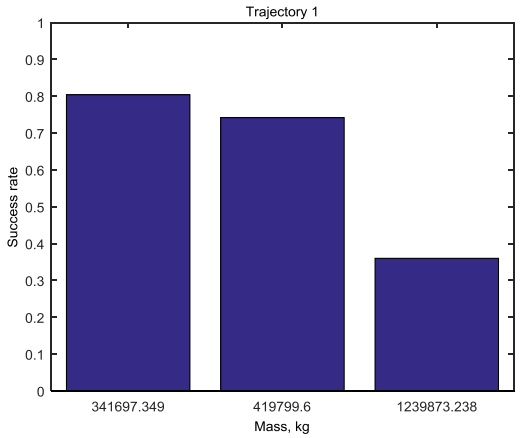
Trajectory 1
Success rate
Mass, kg
341697.349
419799.6
1239873.238

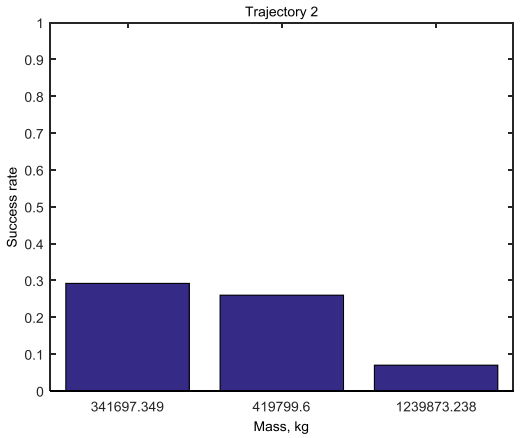
Trajectory 2
Success rate
Mass, kg
341697.349
419799.6
1239873.238

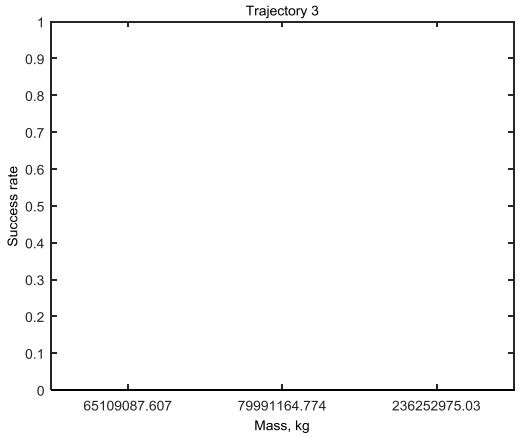
Trajectory 3
Success rate
Mass, kg
65109087.607
79991164.774
236252975.03

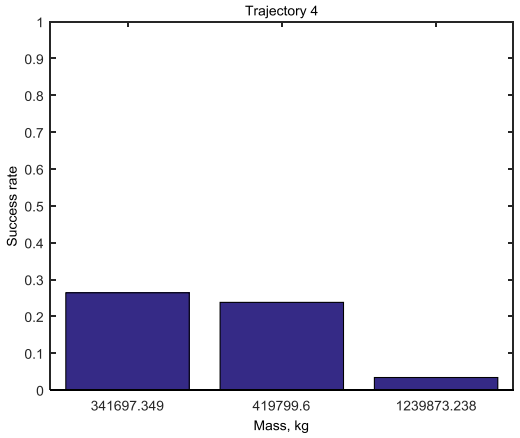
Trajectory 4
Success rate
Mass, kg
341697.349
419799.6
1239873.238

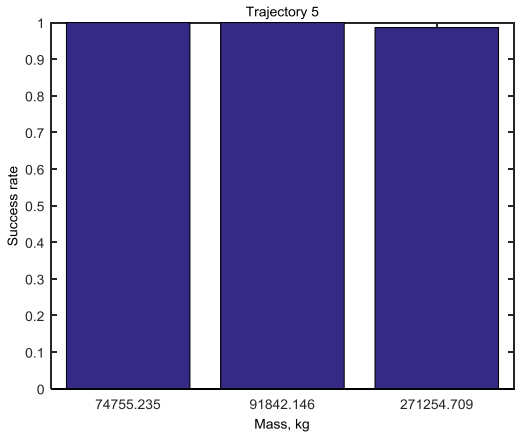
Trajectory 5
Success rate
Mass, kg
74755.235
91842.146
271254.709

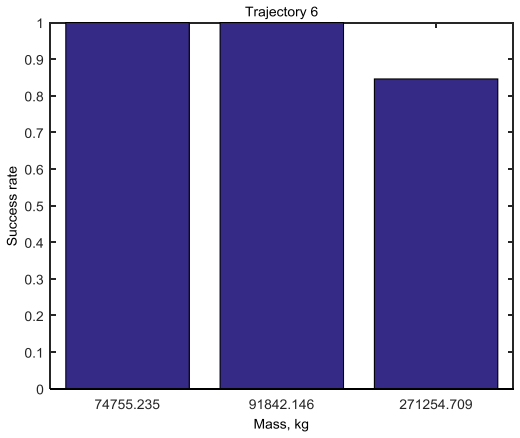
Trajectory 6
Success rate
Mass, kg
74755.235
91842.146
271254.709

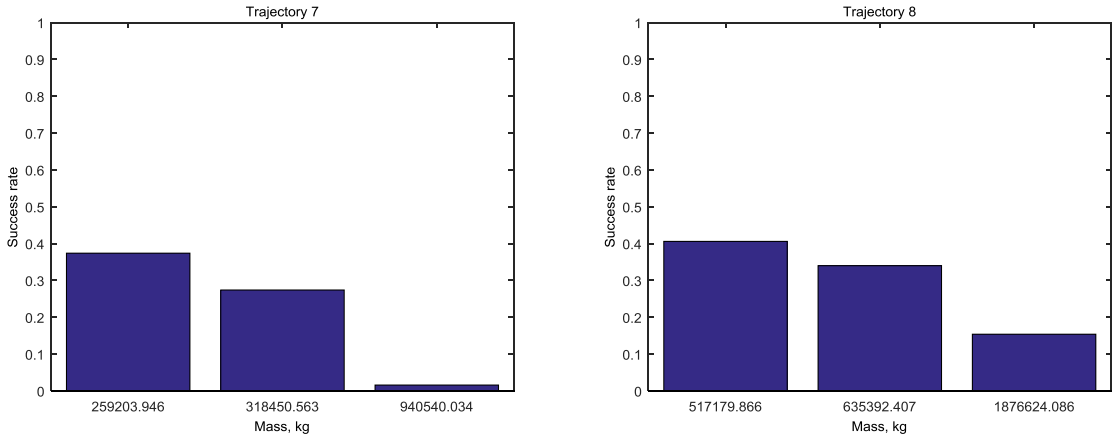

Fig. 11. Success rate of Monte Carlo simulation of the control. Each plot refers to one trajectory, and it includes the success rate for three different asteroid masses.

In order to uncouple the effect of the asteroid's mass on the response of the feedback control performance for a given trajectory, another set of Monte Carlo simulations was run: this time, the same value of mass was used for all the trajectories: 170,169 kg, corresponding to a spherical standard asteroid (ρ = 2,600 kg/m^3) of 5 m of diameter. The results for this set of simulations are presented in Fig. 12.

This second simulation allows to see that, for example, trajectory 3 has an 80% success rate, higher than trajectories 2, 4 and 7. We can therefore conclude that the controllability of trajectory 3 itself is in fact higher than others, however the huge mass of the asteroid 2000SG344 associated to this trajectory makes it unfeasible, as discussed previously.

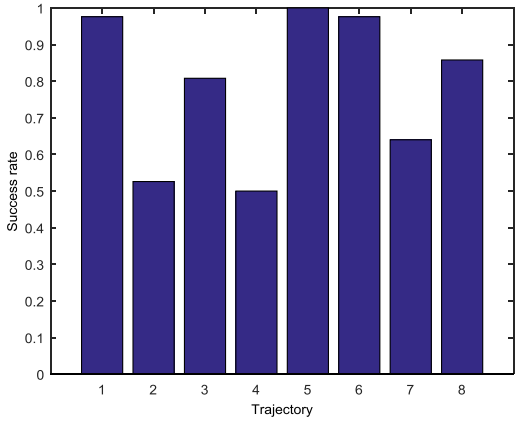

Fig. 12. Success rate of Monte Carlo simulation of the control, assuming asteroid mass 170,169 kg for all the trajectories.

5.1. Required thrust for each asteroid

As mentioned, the results in the previous Section 5 were found assuming the same maximum available thrust level for the shepherding spacecraft. This assumption is based both on the fact that an asteroid's mass will be unknown until proximity measurements, and possibly Δv maneuvers, are performed, and on the fact that there are physical and engineering limitations on the size, mass and power of the spacecraft, which in turn limit the thrust level.

It is however interesting to study the thrust level necessary to guarantee the controllability of the asteroids on their own trajectories; for this, we considered each asteroid to have their own estimated mass (i.e. standard NEA density) The maximum available thrust T_{max} was varied until the success rate of 100 Monte Carlo runs was above 95%, following a Newton-Raphson scheme. Note that because the maximum available thrust changes, a GA optimization to find the best LQR weights was run for each tentative value of T_{max}.

Results are shown in Fig. 13. The right vertical axis in the plot shows the required T_{max}, while the left one shows the scale with respect to the nominal maximum thrust of 1.9 N proposed previously in Section 4. For example, the asteroid on trajectory 4 would require a spacecraft capable to deliver 19 N of maximum thrust (i.e. 10 times the nominal thrust assumed earlier) to achieve 95% of success rate. Conversely, asteroids in trajectories 5 and 6 would only require a fraction of the nominal maximum thrust originally allocated.

These results are consistent with the previous ones, in that lower success rates with the nominal maximum thrust are associated to higher maximum thrust required to reach 95% of success rate.

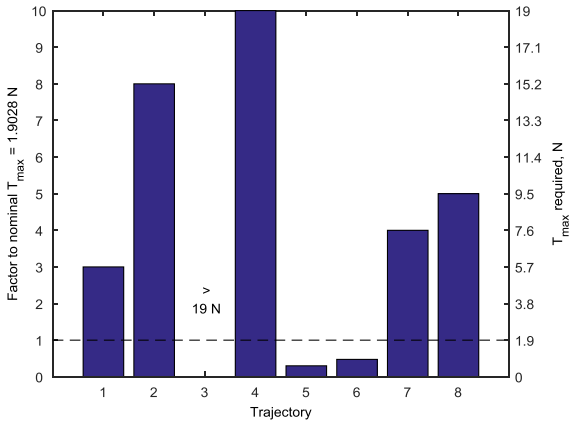

Fig. 13. Maximum thrust necessary to achieve success rate of at least 95% (trajectory 3 requires a thrust > 19 N and is not plotted).

5.2. Comparison of analytical stability with numerical simulations

In subsection 2.3 we discussed the stability of the trajectories using an analytical approach. Those results apparently seem to differ with respect to what was found using the numerical LQR controller through the Monte Carlo simulations. For example, Fig. 11 revealed that trajectory 3 had the lowest success rate (zero), however according to the analytical stability (recall Fig. 6b), trajectory 3 is not the most unstable one; the numerical results showed that trajectory 5 is the most reliable, with a success rate close to unity, however the same trajectory has a relatively low stability indicator as in Fig. 6b. This apparent contradiction can be explained considering that the Monte Carlo simulations account for the mass of the asteroid (in respect to the available thrust) and the different values of uncertainties on the initial states for each trajectory (as in Table 2): instead, the analytical indicator η provides only a measure of the stability of the flux in the vicinity of the trajectory, and neither does it consider the acceleration

available (which in turn depends on the maximum thrust and the asteroid mass) nor the uncertainty on the initial states.

Even if we consider the results in Fig. 12, where the success rate is computed using the same asteroid mass for all the trajectories, it is difficult to identify a correlation with the analytical indicator in Fig. 6b. This is once more due to the fact that results in Fig. 6 do not account for different initial uncertainties in the initial states.

To back up these statements, a further Monte Carlo simulation was run, assuming the same mass for all the asteroids, as in Fig. 12, but this time also using the same uncertainty for the initial state: this has been set to the average value over all the trajectories, as in Table 2. The success rate of this simulation is displayed on the dark blue bars in Fig. 14. To show that now this success rate reflects the result in the analytical stability, we remind that the indicator η is higher for unstable orbits, which should correspond to low values of success rate, and vice versa. In order to compare these measures with opposite meaning, light gray bars in Fig. 14 show a modified indicator, where the maximum value of η_i over all trajectories *i* has been used for normalization, and then the difference to one has been plotted, to invert the stable/unstable meaning. In formulas:

$$1-\frac{\eta_i}{\max_i\left[\eta_i\right]}, \qquad i=1...8\,.$$

This modified indicator can now be compared with the success rate, and similar qualitative trends can now be observed between the analytical stability of these trajectories and the success rates of the control algorithm. Once again, it is important to underline the qualitative – and not quantitative – meaning of the analytical indicator: this is due to the linear approach it relies on, and therefore inherently becomes less reliable with longer or highly-unstable trajectories. For example, focusing on trajectory 7, the indicator predicted high instability: while the numerical value of the indicator is quite far from the success rate of the Monte Carlo approach, partly also because of the normalization used, it has nonetheless predicted that this trajectory is the hardest to control compared to the others.

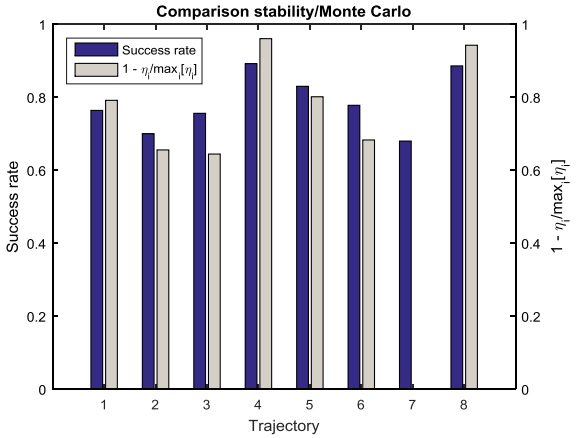

Fig. 14. Success rate of Monte Carlo simulation of the control, assuming same asteroid mass and uncertainty on initial state for all the trajectories (dark blue bars); normalized stability indicator (light grey bars).

6. CONCLUSIONS

This paper demonstrates that the control of asteroids along hyperbolic trajectories leading to the Earth neighborhood, as well as along periodic orbit near the collinear equilibrium points, is a very complex problem. This complexity lies in the heterogeneity of the multiple factors that drive the ultimate controllability of a retrieval trajectory.

The results presented here showed that some combinations of trajectory/asteroid could not be controlled with the proposed propulsion technology and that much higher thrust would therefore be required to ensure the safety of the retrieval mission. Vice-versa, the Monte Carlo simulation showed that some other combinations are very robust, and that the asteroid can be controlled even in case of large errors during insertion maneuvers. It is clear then that the size of the asteroid plays a paramount role in the controllability given a fixed thrust level, but also the costs and length of the insertion maneuvers, since uncertainties are propagated along the insertion trajectories. Finally, the results show also that the hyperbolic trajectories and the final periodic orbits themselves have intrinsic stability properties that play an important part in the overall controllability of the mission.

Hence, given the hazard that an uncontrolled NEO could potentially pose to the Earth, this paper has shown that the controllability of the system should therefore be one of the key parameters when designing an asteroid retrieval mission. Candidate asteroid, insertion maneuver and final target asteroid should then be robustly designed in order to maximize the likelihood of mission success.

ACKNOWLEDGEMENTS

J. P. Sanchez would like to acknowledge the support of the European Commission under the Marie Curie grant 330649 (AsteroidRetrieval). The authors would like to thank J. M. Modelo for his technical insights into the stability of the hyperbolic and periodic trajectories.

NOMENCLATURE

A	Matrix of partial derivatives of the dynamical system with respect the states (i.e. Jacobian)
B	Matrix of partial derivatives of the dynamical system with respect the controls
g_0	Standard gravity acceleration, m/s^2
H	Absolute magnitude
I	Identity matrix
I_{sp}	Specific impulse, s
I_{tran}	Change of linear momentum
J	Cost function
K	Control gain matrix
M	Monodromy matrix
m	Mass, kg
m_{ast}	Asteroid mass, kg
$m_{\text{s/c}}$	Spacecraft mass, kg
N	Number of trials
$P_{SEP,max}$	Spacecraft power, kW
p	Success rate
p_v	Asteroid's albedo
Q	State weights in cost function
R	Control weights in cost function
r	Position vector in the synodic frame
r_E	Distance to the Earth
r_S	Distance to the sun
s	State vector of a reference trajectory
t	Time
t_0	Initial time
T	Period of a periodic orbit
T_{max}	Maximum thrust, N
T_x, T_y, T_z	Thrust components, N
u	Control vector
v	Velocity vector in the synodic frame
$\delta\mathbf{s}$	Error in state **s**, km and km/s
Δv	Change in velocity, m/s
δm_{ast}	Error in the asteroid mass, kg
δv_{tran}	Error in velocity
η	Average expansion of a hyperbolic trajectory
η_{PO}	Average expansion of a periodic orbit

η_{SEP}	Efficiency of the solar electric propulsion system
x, y, z	Components of position vector in synodic frame
$\lambda_{\mathbf{B}}$	Eigenvalue of matrix **B**
μ	Mass parameter of the circular restricted three-body problem
ρ	Asteroid density, kg/m^3
σ	Standard deviation
$\mathbf{\Phi}$	State transition matrix
Ω	Potential function of the circular restricted three-body problem

REFERENCES

[1] V. Badescu, Asteroids - Prospective Energy and Material Resources, Springer-Verlag, Berlin Heidelberg, 2013. DOI: 10.1007/978-3-642-39244-3.

[2] J.S. Lewis, Mining the sky: untold riches from the asteroids, comets and planets, Helix Books/Perseus Books, Reading, Massachusetts, USA, 1996.

[3] C. Lewicki, P. Diamandis, E. Anderson, C. Voorhees, F. Mycroft, Planetary Resources—The Asteroid Mining Company, New Space, 1 (2013) 105-108. DOI: 10.1089/space.2013.0013.

[4] H.-X. Baoyin, Y. Chen, J.-F. Li, Capturing near earth objects, Research in Astronomy and Astrophysics, 10 (2010) 587-598. DOI: 10.1088/1674-4527/10/6/008.

[5] J.P. Sanchez, C.R. McInnes, Asteroid resource map for near-Earth space, J Spacecraft Rockets, 48 (2011) 153-165. DOI: 10.2514/1.49851.

[6] Z. Hasnain, C.A. Lamb, S.D. Ross, Capturing near-Earth asteroids around Earth, Acta Astronaut, 81 (2012) 523-531. DOI: 10.1016/j.actaastro.2012.07.029.

[7] J. Brophy, C. Fred, L. Friedman, Asteroid retrieval feasibility study, Keck Institute for Space Studies, California Institute of Technology, Jet Propulsion Laboratory, Pasadena, California, 2012.

[8] N. Lladó, J.J. Masdemont, G. Gómez, Y. Ren, Capturing small asteroids into the Sun-Earth Lagrangian L1, L2 points for mining purposes, 63rd International Astronautical Congress (IAC 2012), IAF, Naples, Italy, 2012.

[9] D. García Yárnoz, J.P. Sanchez Cuartielles, C.R. McInnes, Easily retrievable objects among the NEO population, Celest Mech Dyn Astr, 116 (2013) 367-388. DOI: 10.1007/s10569-013-9495-6.

[10] R.H. Battin, An introduction to the mathematics and methods of astrodynamics, Revised edition ed., AIAA, New York, 1999.

[11] C.C. Conley, Low Energy Transit Orbits in the Restricted Three-Body Problems, SIAM Journal on Applied Mathematics, 16 (1968) 732–746. DOI: 10.1137/0116060.

[12] M. Ceriotti, J.P. Sanchez Cuartielles, Orbit control of asteroids in libration point orbits for resource exploitation, 64th International Astronautical Congress (IAC 2013), IAF, Beijing, China, 2013.

[13] V. Szebehely, Theory of Orbits: The Restricted Problem of Three Bodies, Academic Press, 1963.

[14] G. Gómez, À. Jorba, J.J. Masdemont, C. Simó, Study of the transfer from the Earth to a halo orbit around the equilibrium pointL 1, Celest Mech Dyn Astr, 56 (1993) 541-562. DOI: 10.1007/BF00696185.

[15] D.A. Vallado, Fundamentals of Astrodynamics and Applications, 3rd Edition ed., Microcosm Press/Kluwer Academic Publishers, El Segundo, California, 2007.

[16] R. Thurman, P.A. Worfolk, The geometry of halo orbits in the circular restricted three-body problem, 1996.

[17] S. Wiggins, Introduction to applied nonlinear dynamical systems and chaos, Springer Science & Business Media, 2003.

[18] J. Stoer, R. Bulirsch, Introduction to numerical analysis, Springer Science & Business Media, 2013.

[19] A. Fujiwara, J. Kawaguchi, D.K. Yeomans, M. Abe, T. Mukai, T. Okada, J. Saito, H. H. Yano, M. Yoshikawa, D.J. Scheeres, O. Barnouin-Jha, A.F. Cheng, H. Demura, R.W. Gaskell, N. Hirata, H. H. Ikeda, T. Kominato, H.

Miyamoto, A.M. Nakamura, R. Nakamura, S. Sasaki, K. Uesugi, The Rubble-Pile Asteroid Itokawa as Observed by Hayabusa, Science, 312 (2006) 1330-1334.
[20] E. Bowell, B. Hapke, D. Domingue, K. Lumme, J. Peltoniemi, A.W. Harris, Application of photometric models to asteroids, in: R.P. Binzel, R.P. Gehrels, M.S. Matthews (Eds.), Asteroids II, Univ. of Arizona Press, Tucson, AZ, USA, 1989, pp. 524–556.
[21] S.R. Chesley, P.W. Chodas, A. Milani, D.K. Yeomans, Quantifying the Risk Posed by Potential Earth Impacts, Icarus, 159 (2002) 423-432. DOI: 10.1006/icar.2002.6910.
[22] S.R. Chesley, P.W. Chodas, A. Milani, G.B. Valsecchi, D.K. Yeomans, Quantifying the Risk Posed by Potential Earth Impacts, Icarus, 159 (2002) 423-432. DOI: 10.1006/icar.2002.6910.
[23] P. McCullagh, J. Nelder, Generalized Linear Models, Second Edition, Springer-Science+Business Media, B.V., 1989.
[24] A.E. Bryson, Y.-C. Ho, Applied optimal control: optimization, estimation, and control (Revised printing), Taylor & Francis Group, New York, 1975.
[25] M. Ceriotti, C.R. McInnes, Hybrid solar sail and solar electric propulsion for novel Earth observation missions, Acta Astronaut, 69 (2011) 809–821. DOI: 10.1016/j.actaastro.2011.06.007.
[26] S. Kitamura, Y. Ohkawa, Y. Hayakawa, H. Yoshida, K. Miyazaki, Overview and research status of the JAXA 150-mN ion engine, Acta Astronaut, 61 (2007) 360-366. DOI: 10.1016/j.actaastro.2007.01.010.

Vitae

MATTEO CERIOTTI

Dr. Matteo Ceriotti received his M.Sc. summa cum laude from Politecnico di Milano (Italy) in 2006 with a thesis on planning and scheduling for planetary exploration. In 2010, he received his Ph.D. on "Global Optimisation of Multiple Gravity Assist Trajectories" from the Department of Aerospace Engineering of the University of Glasgow (United Kingdom). During 2009-2012, Matteo was a research fellow at the Advanced Space Concepts Laboratory, University of Strathclyde, Glasgow, leading the research theme "Orbital Dynamics of Large Gossamer Spacecraft". In 2012, he returned to the University of Glasgow as a lecturer in Space Systems Engineering, within the School of Engineering. His main research interests are space mission analysis and trajectory design, orbital dynamics, trajectory optimization, particularly focusing on high area-to-mass ratio structures.

JOAN PAU SANCHEZ

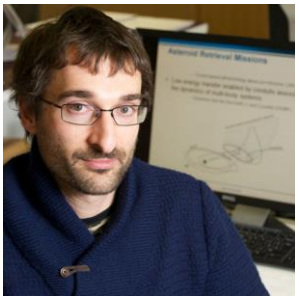

Dr. Joan-Pau Sánchez studied physics at the Universitat de Barcelona, and an MSc in Mission Analysis and Design at the University of Glasgow. He was awarded his PhD also from University of Glasgow in 2009, after completing a comprehensive analysis of deflection alternatives against Earth-threatening asteroids. He then briefly worked as space mission analysis at GMV Aerospace and Defence, before returning to academia. He joined the University of Strathclyde as postdoctoral research fellow, leading the Visionary Space Systems theme within the ERC project VISIONSPACE. In 2012, he was granted an individual Marie Curie Fellowship to pursue his research on asteroid retrieval missions at the Universitat Politècnica de Catalunya. He joined Cranfield University on February 2015 as lecturer in Space Engineering. He is particularly active in the research fields of small body missions and space macro engineering projects.